

A terahertz pulse emitter monolithically integrated with a quantum cascade laser

David Burghoff,^{1,a)} Tsung-Yu Kao,¹ Dayan Ban,² Alan Wei Min Lee,¹ Qing Hu,¹ and John Reno³

¹Department of Electrical Engineering and Computer Science, Research Laboratory of Electronics, Massachusetts Institute of Technology, Cambridge, Massachusetts 02139, USA

²Department of Electrical and Computer Engineering, University of Waterloo, Waterloo N2L 3G1, Canada

³Department 1123, Sandia National Laboratories, MS 0601, Albuquerque, New Mexico 87185-0601, USA

(Received 23 December 2010; accepted 18 January 2011; published online 11 February 2011)

A terahertz pulse emitter monolithically integrated with a quantum cascade laser (QCL) is demonstrated. The emitter facet is excited by near-infrared pulses from a mode-locked Ti:sapphire laser, and the resulting current transients generate terahertz pulses that are coupled into an electrically isolated QCL in proximity. These pulses are used to measure the gain of the laser transition at ~ 2.2 THz, which clamps above threshold at ~ 18 cm⁻¹ and has a full width at half-maximum linewidth of ~ 0.67 THz. The measurement also shows the existence of absorption features at different biases that correspond to misalignment of the band structure and to absorption within the two injector states. The simplicity of this scheme allows it to be implemented alongside standard QCL ridge processing and to be used as a versatile tool for characterizing QCL gain media. © 2011 American Institute of Physics. [doi:10.1063/1.3553021]

In the past few years, terahertz time-domain spectroscopy (TDS) has become the method of choice for characterizing terahertz quantum cascade laser (QCL) gain media, on account of its unique ability to identify both the amplitude and phase associated with intersubband transitions.¹ Recent work has demonstrated the presence of linewidth narrowing,² spatial hole burning,³ and absorption features associated with transitions other than the one that produces lasing.⁴ Typically, terahertz radiation is generated externally with a photoconductive antenna, focused onto one QCL facet, transmitted through the waveguide, collected from the other facet, and detected through photoconductive or electro-optic means. Because this process leads to low coupling efficiencies, only QCLs with single plasmon waveguide geometries—which have large modes and a Fresnel-like impedance mismatch to free space—have been characterized with this method. However, metal-metal waveguides have largely supplanted the surface plasmon waveguide in terahertz QCL research, as their tighter confinement of the optical mode leads to a near-unity overlap with the active region and reduced mirror losses,⁵ resulting in much higher maximum operating temperatures.⁶ On the other hand, these very properties make coupling efficiencies to and from the waveguide with an external terahertz pulse emitter low, thereby making TDS difficult to perform.

Several schemes have been proposed to overcome the small coupling efficiency of terahertz radiation into metal-metal waveguides, including the integration of horn antennas⁷ and the affixation of hyperhemispherical lenses to the QCL facet.⁸ One of the most promising methods demonstrated is the generation of terahertz pulses at the facet itself via photoconductive means, in which femtosecond near-infrared (NIR) pulses impinge directly onto the facet and terahertz pulses are generated by the resulting current transient.^{9,10} However, since the pulse amplitude (and possi-

bly its frequency dependence) depends on the QCL bias, on-facet intracavity generation fundamentally couples the generation process of the terahertz pulse to the amplification process of the QCL, making it difficult to determine how the pulse is modified by the active region. By the same token, the excitation affects the QCL: free electrons generated by NIR excitation have been shown to increase the loss of the waveguide,⁹ and voltage transients generated by instantaneous shorting can affect the QCL bias.¹¹ In this letter, we demonstrate a simple but effective method in which a separate photoconductive emitter section is fabricated from the QCL ridge itself, with the emitter and laser ridge separated by a short air gap. Because the emitter is well-matched to the QCL, the generated pulse couples to the QCL with a high efficiency. Moreover, since the emitter can be independently biased, an unambiguous determination of the active region's effect on the generated pulse can be made.

The inset of Fig. 1 shows a basic diagram of the struc-

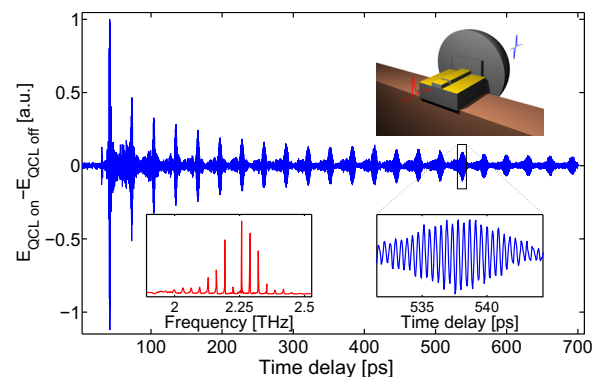


FIG. 1. (Color online) Difference field propagating through the QCL above threshold. The delay stage used has only 25 mm of travel distance, so five separate scans were stitched together. The top-right inset shows a basic schematic of the emitter and QCL. The bottom-left inset shows a power spectrum (Fourier transform magnitude-squared) of the difference field. The bottom-right inset shows a zoomed-in view of the 16th echo and the corresponding time-domain oscillations.

^{a)}Electronic mail: burghoff@mit.edu.

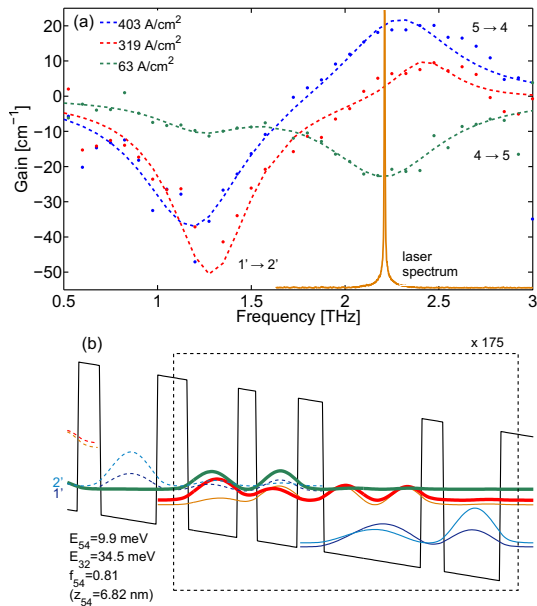


FIG. 2. (Color online) (a) Measured gain at different biases (dots) with double-Lorentzian fits (lines). Peaks are labeled with the corresponding transitions. The lasing spectrum of a similar device is shown for reference. (b) Band diagram of the device measured. Starting from the left injection barrier, layer thicknesses in angstrom are **51/82/31/68/42/161/37/93**, with the bold fonts representing barriers. The 161 Å well is bulk-doped to $1.9 \times 10^{16} \text{ cm}^{-3}$, resulting in a $3 \times 10^{10} \text{ cm}^{-2}$ sheet density per module.

ture that was fabricated. The gap that separates the emitter section from the laser section was defined lithographically with the same plasma etch that creates the QCL ridge, and is $\sim 4 \mu\text{m}$ wide. The emitter section was fabricated to be 100 μm long, but was subsequently cleaved to $\sim 15 \mu\text{m}$ in order to reduce the effects of Fabry-Pérot fringes within the emitter. Not shown is the bonding pad used to bias the emitter, which was formed by masking a QCL ridge with a silicon dioxide layer before deposition of the top metallic contact. An aplanatic silicon hyperhemispherical lens was affixed to the back facet of the QCL in order to improve outcoupling of the terahertz pulse;⁸ the use of this lens is critical for obtaining the high signal-to-noise ratios in the results reported here. Devices of varying widths and lengths were tested, but the device comprising the data shown in this letter is 1.21 mm long and 80 μm wide. The QCL active region itself—design FL175M-M3, shown in Fig. 2(b)—is a resonant-phonon design that lases at $\sim 2.2 \text{ THz}$. It has a two-well injector region and is similar to the design described in Ref. 12.

Near-infrared pulses were generated from a mode-locked Ti:sapphire laser with a pulse width of $\sim 80 \text{ fs}$, a repetition rate of 80 MHz, and a center wavelength of 790 nm, chosen to maximize the amplitude of the generated terahertz pulse. The 125 mW pump pulse was then focused onto the emitter facet to a spot size of about 20 μm . The choice of such a large spot size compared to the QCL height (10 μm) helped to reduce the effect of mechanical oscillations induced by our pulsed-tube cryostat, which cooled the QCL to $\sim 33 \text{ K}$. Radiation was collected out of the device and focused onto a 1 mm thick ZnTe crystal with a pair of $f/2.5$ off-axis parabolic mirrors, and standard electro-optic sampling¹³ was performed to detect the electric field as a function of probe delay. As in Ref. 10, the peak field scaled approximately linearly in the emitter bias, and although a

reverse-biased emitter produced a peak field similar in magnitude to a forward-biased emitter, it also minimized dark current. This aspect of the reverse bias, together with the modest choice of pump power, allowed similar emitters to be biased as high as -50 V before device failure sets in. For this measurement, the emitter was square-wave modulated at 50 kHz from -16 to $+1 \text{ V}$, and the QCL was independently modulated at 27 kHz with 10% duty cycle. The balanced detector output was fed into a lock-in amplifier tuned to the 50 kHz emitter signal, and the demodulated but unfiltered output of this amplifier was fed into a second lock-in tuned to the 27 kHz QCL signal. Data is recorded from both lock-ins simultaneously: The first is sensitive to the generated terahertz field time-averaged over the QCL's bias period, while the second is sensitive only to the difference of the terahertz field induced by the QCL bias. By polling each as we scan the delay stage and digitally processing the result, we can simultaneously determine what the transmitted pulse would be if the QCL were completely on and what it would be if it were completely off. Although we could in principle also do this by adding the difference signal to a separate reference scan taken with the QCL simply off,¹⁴ our method allows us to compensate for cryostat-induced long-term drift of the QCL position that effectively changes the NIR power incident on the facet. For cleaved emitters, the terahertz spectrum obtained with the QCL off is similar to the unamplified spectra in Ref. 9, with a signal-to-noise ratio of 50 dB at 2.2 THz and a bandwidth of 3 THz (likely limited by our femtosecond laser and sampling crystal).

Figure 1 shows the difference signal (i.e., the readout of the second lock-in amplifier) passed through a QCL biased above threshold as a function of delay. Since energy at the lasing frequency suffers zero loss while nearby frequencies do not, the initial pulse generated by the emitter gives rise to dozens of echoes that correspond to the round-trip time of the cavity, 31 ps, and narrow to the lasing frequency as they circulate in the cavity. From this round-trip time, we can estimate that the waveguide has a group index of 3.84. In addition, we note the presence of a small pulse that appears 11.2 ps before the main pulse, which we attribute to a mode with a group index of 1.07. This near-vacuum index is a strong indicator that the signal is from one of the air-side modes described in Ref. 10; careful alignment of the aplanatic lens helps to significantly reduce this mode relative to the desired waveguide modes. Lastly, note that the power spectral density of the difference pulse shows a uniformly spaced comb, indicating that only one lateral mode was excited by the terahertz pulse. Moreover, the frequency range in which longitudinal modes are visible is the same range that has appreciable gain [see Fig. 2(a)].

Figure 2(a) shows the measured gain as a function of frequency and at several bias points. (The method used to determine gain is similar to that used in Ref. 14; gain was calculated using a 13.3 ps Hamming window that excludes the air-side mode and reflections within the ZnTe sampling crystal.) Also shown on each curve is a double-Lorentzian fit to the measured data. At 63 A/cm², far below the lasing threshold of $\sim 360 \text{ A/cm}^2$, the current begins to rise quickly with the bias voltage, and we observe an absorption feature that we attribute to an alignment of the injector states to the lower laser level (similar to what was seen in Ref. 4), resulting in absorption at the lasing frequency rather than gain. We also observe a weak absorption at $\sim 1.25 \text{ THz}$ that is likely

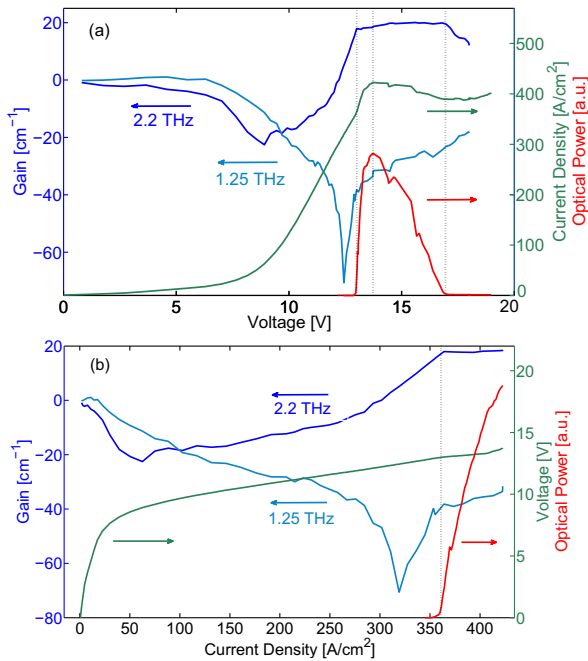


FIG. 3. (Color online) (a) Gain at 2.2 THz, gain at 1.25 THz, light output, and current density as functions of QCL voltage bias. The three dotted vertical lines indicate the onset of lasing, the onset of NDR, and the cessation of lasing. (b) Gain, light output, and voltage as functions of QCL current bias. Dotted vertical line indicates the onset of lasing. (NDR regime has been suppressed for clarity).

due to absorption between the two injector states. The only other transition with a comparable energy is between levels 3 and 4, but because electrons in state 3 can quickly emit an LO phonon while the injection barrier represents a transport bottleneck, we expect the population of state 1' to be significantly higher than the population of state 3. At 319 A/cm², still below threshold, the upper laser level is being populated, and gain is observed near 2.2 THz. The absorption between the injector states has become stronger because of a greater wavefunction overlap. Finally, at 403 A/cm² (above threshold), the gain at 2.2 THz has become sufficient to enable lasing, and it clamps at ~ 18 cm⁻¹ with a full width at half-maximum of approximately 0.67 THz. It is also apparent that the gain spectrum is asymmetric, with the lower-frequency side dragged down by the 1' \rightarrow 2' absorption. This intra-injector absorption will become more severe at lower lasing frequencies, and this is the very reason that a one-well injector scheme was developed for low-frequency resonant-phonon terahertz QCLs.¹⁵

Figures 3(a) and 3(b) show the measured gain (or loss) at 2.2 and 1.25 THz as a function of voltage and as a function of current, respectively, with the overlay of current-voltage (voltage-current) and power-voltage (power-current) curves shown for comparative analysis. When the structure is unbiased, there is no absorption or gain between the lasing levels because there is no population in the lasing pair of levels 4 and 5. However, once the structure is sufficiently voltage-biased, the injector is aligned to the lower laser level 4, and absorption turns on. In fact, absorption turns on almost immediately once current begins to flow, showing that conduction within the active region at this temperature cannot occur without transport through the lasing states. As voltage is in-

creased further, the upper laser level is populated instead of the lower one, and the absorption yields to gain. At the same time, the absorption at 1.25 THz *drops*, suggesting that the population inversion has come about through the depopulation of injector state 1': Resonant tunneling is now occurring. Eventually, the laser threshold is reached, and the gain clamps to the total losses of the cavity, ~ 18 cm⁻¹. As bias is increased to the negative differential resistance (NDR) point, the gain slightly unclamps, as electrical instability has effectively decreased the amount of time the laser is on. Finally, lasing is disabled once the structure is sufficiently biased that the gain drops below threshold.

In conclusion, we have demonstrated the integration of an independent terahertz pulse generator with a QCL gain medium in a way that is compatible with a standard QCL ridge based on a metal-metal waveguide. We have used this integrated structure to measure the gain and absorption of these QCLs and to unambiguously show the presence of several absorption features both below and above threshold. As demonstrated here, this method could yield high-quality results that have been elusive so far in QCLs with metal-metal waveguides, and it could prove to be an invaluable technique for characterizing gain media designs.

This work was supported by NASA and NSF. Sandia is a multiprogram laboratory operated by Sandia Corporation, a Lockheed Martin Co., for the U.S. Department of Energy under Contract No. DE-AC04-94AL85000. The authors would also like to thank Qi Qin and Sushil Kumar for their assistance in fabricating other devices used in this project.

- ¹J. Kröll, J. Darmo, S. S. Dhillon, X. Marcadet, M. Calligaro, C. Sirtori, and K. Unterrainer, *Nature (London)* **449**, 698 (2007).
- ²N. Jukam, S. S. Dhillon, D. Oustinov, Z. Zhao, S. Hameau, J. Tignon, S. Barbieri, A. Vasanelli, P. Filloux, C. Sirtori, and X. Marcadet, *Appl. Phys. Lett.* **93**, 101115 (2008).
- ³J. Kröll, J. Darmo, K. Unterrainer, S. S. Dhillon, C. Sirtori, X. Marcadet, and M. Calligaro, *Appl. Phys. Lett.* **91**, 161108 (2007).
- ⁴N. Jukam, S. S. Dhillon, D. Oustinov, J. Madéo, J. Tignon, R. Colombelli, P. Dean, M. Salih, S. P. Khanna, E. H. Linfield, and A. G. Davies, *Appl. Phys. Lett.* **94**, 251108 (2009).
- ⁵B. S. Williams, S. Kumar, H. Callebaut, Q. Hu, and J. L. Reno, *Appl. Phys. Lett.* **83**, 2124 (2003).
- ⁶S. Kumar, Q. Hu, and J. L. Reno, *Appl. Phys. Lett.* **94**, 131105 (2009).
- ⁷J. Lloyd-Hughes, G. Scalari, A. van Kolck, M. Fischer, M. Beck, and J. Faist, *Opt. Express* **17**, 18387 (2009).
- ⁸A. W. M. Lee, Q. Qin, S. Kumar, B. S. Williams, Q. Hu, and J. L. Reno, *Opt. Lett.* **32**, 2840 (2007).
- ⁹S. S. Dhillon, S. Sawallich, N. Jukam, D. Oustinov, J. Madéo, S. Barbieri, P. Filloux, C. Sirtori, X. Marcadet, and J. Tignon, *Appl. Phys. Lett.* **96**, 061107 (2010).
- ¹⁰M. Martl, J. Darmo, D. Dietze, K. Unterrainer, and E. Gornik, *J. Appl. Phys.* **107**, 013110 (2010).
- ¹¹N. Jukam, S. S. Dhillon, D. Oustinov, J. Madéo, C. Manquest, S. Barbieri, C. Sirtori, S. P. Khanna, E. H. Linfield, A. G. Davies, and J. Tignon, *Nat. Photonics* **3**, 715 (2009).
- ¹²B. Williams, S. Kumar, Q. Hu, and J. Reno, *Electron. Lett.* **40**, 431 (2004).
- ¹³Q. Wu and X. Zhang, *Appl. Phys. Lett.* **67**, 3523 (1995).
- ¹⁴N. Jukam, S. Dhillon, Z. Y. Zhao, G. Duerr, J. Armijo, N. Simons, S. Hameau, S. Barbieri, P. Filloux, C. Sirtori, X. Marcadet, and J. Tignon, *IEEE J. Sel. Top. Quantum Electron.* **14**, 436 (2008).
- ¹⁵S. Kumar, B. S. Williams, Q. Hu, and J. L. Reno, *Appl. Phys. Lett.* **88**, 121123 (2006).